

# Angularly Selective Enhanced Vortex Screening in Extremely Layered Superconductors with Tilted Columnar Defects

Gonzalo Rumi,<sup>1,2,3,4</sup> Vincent Mosser,<sup>5</sup> Marcin Konczykowski,<sup>6</sup> and Yanina Fasano<sup>1,2,3</sup>

<sup>1</sup>*Low Temperatures Lab, Centro Atómico Bariloche, CNEA, Argentina.*

<sup>2</sup>*Instituto de Nanociencia y Nanotecnología, CONICET-CNEA, Nodo Bariloche, Argentina.*

<sup>3</sup>*Instituto Balseiro, CNEA and Universidad Nacional de Cuyo, Bariloche, Argentina*

<sup>4</sup>*Neutrons Beam National Lab, CNEA, Argentina*

<sup>5</sup>*Vmmetic SAS, F-75008 Paris, France*

<sup>6</sup>*Laboratoire des Solides Irradiés, CEA/DRF/IRAMIS, École Polytechnique, CNRS, Institut Polytechnique de Paris, F-91128 Palaiseau, France*

(Dated: October 3, 2024)

We report on two mechanisms of angularly selective enhanced screening in the solid vortex phase of extremely layered superconductors with tilted columnar defects (CDs). We study  $\text{Bi}_2\text{Sr}_2\text{CaCu}_2\text{O}_{8+\delta}$  samples with different densities of CD tilted  $45^\circ$  from the  $c$ -axis, and conduct local ac Hall magnetometry measurements, probing the sustainable current of the vortex system. We reveal two types of maxima in sustainable current for particular directions, detected as dips in the magnetic transmittivity of the vortex system. First, for a smaller number of vortices than of defects, an enhancement of screening is detected at an angular location  $\Theta_{\text{dip}}^1 \sim 45^\circ$  for  $H$  applied close to the direction of CD. For a larger number of vortices than of CD,  $\Theta_{\text{dip}}^1$  decreases towards the  $ab$ -plane direction upon warming. Second, a pair of additional dips in transmittivity are detected at angles  $\Theta_{\text{dip}}^2$  closer to, and quite symmetric with, the  $ab$ -plane. These two types of angularly selective enhanced screening reveal the effective pinning by tilted CD even for the composite vortex lattices nucleated in tilted fields in  $\text{Bi}_2\text{Sr}_2\text{CaCu}_2\text{O}_{8+\delta}$ .

## I. INTRODUCTION

In extremely layered superconductors, when the magnetic field is applied tilted with respect to the  $c$ -axis, the vortex lattice results in a compound lattice comprising pancake and Josephson vortices [1–3]. Pancake vortices are confined to the  $\text{CuO}_2$  planes [4, 5] and contain a core within that layer where the superconductivity is depleted. On the other hand, Josephson vortices lack this core structure and are generated by a field component in the  $ab$ -plane [6–8]. The in-plane lattice spacing of the pancake vortices  $a$  is determined by the  $c$ -axis field component and that of the Josephson vortices is given by the in-plane field component. This composite lattice has been revealed by means of vortex imaging techniques [9–12]. Two relevant parameters for the physics of the vortex lattice in these compounds are  $\gamma$ , the electronic anisotropy, and  $s$ , the separation between the  $\text{CuO}_2$  planes. The coupling between pancake vortices of adjacent planes is produced by electromagnetic and Josephson interactions, the latter being dominant when the Josephson length  $\lambda_J = \gamma s$  is smaller than the superconducting penetration depth  $\lambda$ . Layered cuprates present a different balance between these two interactions strongly depending on the oxygen-doping. [13, 14]

This composite nature makes reaching a unified description of vortex matter in layered high- $T_c$  superconductors under tilted fields rather challenging. This basic issue is of crucial relevance for finding paths for enhancing pinning and critical currents. The latter is highly desirable for technological applications, and a good strategy to achieve these conditions is the generation of effective pinning landscapes. To this end, introducing columnar

defects (CDs) produced by heavy-ion irradiation is one of the most effective approaches [15–21].

The case of parallel CD running along the  $c$ -axis (perpendicular to the  $\text{CuO}_2$  planes) has been widely studied in the extremely layered  $\text{Bi}_2\text{Sr}_2\text{CaCu}_2\text{O}_{8+\delta}$  compound that we study here. Their effect on the structural properties of the vortex lattice as well as on the first-order vortex melting transition is vastly reported in the literature. [22–25] These works have settled the general consensus that this type of defect is a very effective pinning center when the field is applied parallel to them. CDs are even more efficient pinning centers when the field is applied in the  $c$ -axis but defects are tilted with respect to this direction since the pinning energy is proportional to the cross-sectional area of the defects in the  $\text{CuO}_2$  planes [20, 26, 27]. Moreover, two sets of crossed CDs tilted with respect to the  $c$ -axis are more efficient to improve the critical current than a parallel set of defects [28, 29]. Thus, the spatial distribution and orientation of CD with respect to the  $\text{CuO}_2$  planes are key for their pinning efficiency [30].

In extremely layered cuprates, when the field is applied tilted from the  $c$ -axis, the pinning of pancake vortices results from the combination of the pinning exerted by CD and by the  $\text{CuO}_2$  planes. Then, the vortex arrangement that minimizes the free energy in different field and temperature ranges is not necessarily that of pancakes located inside CD. In some cases, a staircase vortex configuration [31] can be energetically favorable. It consists of parts of the flux line trapped in different defects, linked by unpinned or weakly pinned segments. In addition, for tilted fields, pancake vortices produce a pinning effect that indirectly affects the dynamics of

Josephson vortices [7].

In order to probe the efficiency of pinning by CD for different field directions in extremely layered cuprates, here, we study the angular dependence of the ac screening of vortex matter in  $\text{Bi}_2\text{Sr}_2\text{CaCu}_2\text{O}_{8+\delta}$  samples with various densities of CDs tilted  $45^\circ$  from the  $c$ -axis. We apply local ac Hall magnetometry in order to obtain information on the sustainable current of the vortex system, a measure of the critical current taking into account creep effects [32]. In particular, we measure the magnetic transmittivity  $T'$  that reflects the sustainable current flowing in the sample for a given ac field  $J = (1/\pi) \arccos(2T' - 1)$  [32]. The angular variation of ac screening has been previously used to reveal the localization of vortices on CDs aligned along the sample  $c$ -axis [33]. The main result of this work is that transmittivity curves are asymmetric and present dips revealing angularly selective enhanced screening. A dip in  $T'$  indicates a maximum in the sustainable current due to increased pinning in the particular angular location. The enhancement of screening is registered close to the direction of CDs, but extra dips at smaller angles are also detected. The detection of a maximum screening in an angular direction not aligned with CDs is unexpected and suggests the existence of staircase pancake vortex configurations that are effectively trapped by tilted CDs.

## II. MATERIALS AND METHODS

Columnar defects were produced in platelet-like optimally doped  $\text{Bi}_2\text{Sr}_2\text{CaCu}_2\text{O}_{8+\delta}$  single crystals grown by the traveling-solvent floating-zone technique [34]. Sub-millimeter size and  $\sim 20 \mu\text{m}$  thick samples were irradiated with 6 GeV Pb ions at GANIL, France. The direction of the beam of ions was rotated from the sample  $c$ -axis in order to create columnar tracks of defects tilted  $45^\circ$  from the  $c$ -axis. The penetration range of the 6 GeV Pb ions largely exceeds the sample thickness divided by the sinus of the tilt angle. The flux of irradiation was chosen to generate various densities of defects corresponding to matching fields when the field is applied in the direction of CDs of  $B_\Phi = 50, 200$  and  $2000 \text{ G}$ , with  $B_\Phi$  as the field value at which the density of CD equals that of the vortices. When the field is applied in the  $c$ -axis direction, the density of the vortices equals that of CDs in a plane parallel to the  $ab$ -plane for a smaller density of  $B_\Phi^c = B_\Phi/\sqrt{2} = 35.5, 141.9$  and  $1419 \text{ G}$ . These densities of CD are such that the separation between defects is smaller ( $B_\Phi = 2000 \text{ G}$ ) and larger ( $B_\Phi = 200, 50 \text{ G}$ ) than  $\lambda_J = \gamma s \sim 0.25 \mu\text{m}$  for  $\text{Bi}_2\text{Sr}_2\text{CaCu}_2\text{O}_{8+\delta}$  with an anisotropy  $\gamma \sim 160$  and a spacing between  $\text{CuO}_2$  planes of  $s = 15 \text{ \AA}$ .

The sample is mounted on top of a chip containing a Hall sensor plus a planar coil. The sample is located with its  $ab$ -plane roughly parallel to the sensor, glued with Apiezon-N grease to improve thermal contact. The component of the local stray field at the

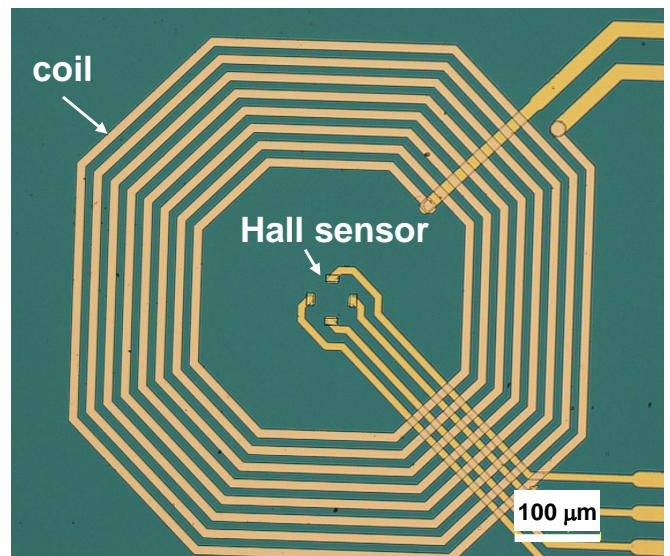


FIG. 1. Hall sensor setup used in the local transmittivity measurements of this work. Detail of the  $10 \times 10 \mu\text{m}^2$  working-area Hall sensor surrounded by an on-chip coil that generates the ripple field for ac measurements. The platelet-like superconducting sample (not shown) is glued with apiezon-N grease parallel to the chip and on top of the Hall probe and the coil. The sensor detects the sample stray field,  $B^\perp$ , pointing in the direction perpendicular to its  $ab$ -plane.

sample surface pointing perpendicular to the  $ab$ -plane,  $B^\perp$ , is detected by a Hall sensor with a  $9 \times 9 \mu\text{m}^2$  working area photolithographically fabricated from a so-called AlGaAs/InGaAs/GaAs pseudomorphic heterostructure with a reduced 2D electron gas density in order to achieve a higher sensitivity amounting to  $\sim 146 \text{ m}\Omega/\text{G}$ . In order to perform ac magnetometry measurements, the sensor is surrounded by an on-chip coil generating the ripple  $h_{ac}$  field. This coil is made up of 8-turn  $0.6 \mu\text{m}$  thin Au film deposited over a silicon oxinitride dielectric layer, with a radius ranging from  $160$  to  $300 \mu\text{m}$  and a pitch of  $20 \mu\text{m}$ . Figure 1 shows a picture of a typical chip containing the Hall sensor and the coil. This chip is then attached into a sample holder that is thermally coupled to the thermometer registering the temperature.

Local magnetic measurements are performed by applying a dc magnetic field  $H$  at an angle  $\theta$  from the  $ab$ -plane of the samples and with a component  $H^\perp$  along the  $c$ -axis; see the insert to Figure 2. The ac transmittivity measurements are performed, applying, in addition, a ripple field  $h_{ac}$  that is parallel to the  $c$ -axis. Angular measurements are performed by sweeping the external magnetic field within the plane defined by the  $c$ -axis and the direction of CDs; see the bottom-left insert to Figure 2. As a consequence, the direction of  $H$  varies, generating a simultaneous sweep of the  $c$ -axis,  $H^\perp$ , and of the  $ab$ -plane components. We perform these measurements in a controlled way using a step motor, allowing us to reach half a degree resolution. Positive  $\theta$  corresponds to angles going from the  $ab$ -plane towards the  $c$ -axis. All mea-

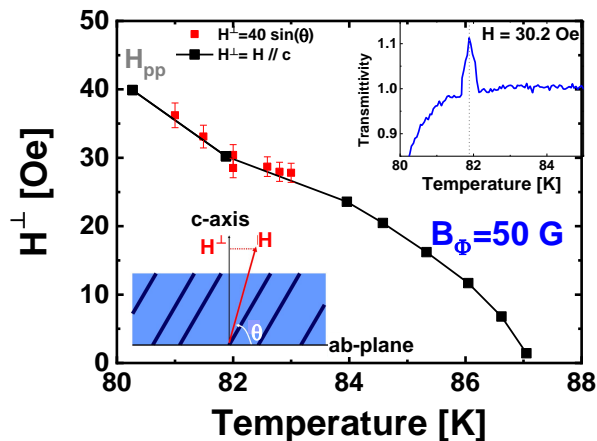


FIG. 2. Phase diagram and angular dependence of transmittivity  $T'$  for a  $\text{Bi}_2\text{Sr}_2\text{CaCu}_2\text{O}_{8+\delta}$  sample with columnar defects with a matching field of  $B_\Phi = 50$  Oe tilted  $45^\circ$  from the  $c$ -axis. First-order melting line  $H_{pp}$  obtained from the location of the paramagnetic peak detected in  $T'$  versus temperature measurements at fixed field (see top insert for example). Black dots correspond to measurements performed with the field applied in the  $c$ -axis direction whereas red dots correspond to the  $c$ -axis component  $H^\perp$  of the field applied at an angle  $\theta$  from the  $ab$ -plane in angular measurements. Top insert:  $T'$  data obtained in the proximity of the paramagnetic peak (dashed line) for 30.2 Oe applied in the  $c$ -axis. Bottom insert: Schematics of the tilted columnar defects (thick black lines) generated at an angle of  $45^\circ$  with respect to the  $c$ -axis and the  $ab$ -plane in a plane running along the long side of the sample. The dc field  $H$  is applied in the plane of the defects at an angle  $\theta$  with respect to the  $ab$ -plane of the sample.

measurements presented here start with the field applied at  $\theta = -90^\circ$  and then the field is rotated counterclockwise towards the  $ab$ -plane with  $\theta = 0$  and finally towards  $\theta = 90^\circ$ .  $h_{ac}$  has a magnitude ranging 0.5–1 Oe rms and frequencies between 0.7 and 1000 Hz.

Hall magnetometry allows the detection of  $B^\perp$ , the local magnetic induction of the sample in the direction perpendicular to the sensors. In ac measurements, we detect the first harmonic of  $B^\perp$  by means of a digital signal-processing lock-in technique. The transmittivity  $T'$  is obtained by normalizing the in-phase component of the first-harmonic signal  $B'$  such that  $T'(T, \theta) = [B'(T, \theta) - B'(T \ll T_c, \theta)] / [B'(T > T_c, \theta) - B'(T \ll T_c, \theta)]$  [35]. Then,  $T' = 1$  in the normal phase for  $T > T_c$  and  $T' = 0$  when full screening takes place at low temperatures well within the superconducting phase. In order to normalize the angular measurements, we first record  $B'(\theta)$  for a given applied  $H$  and for temperatures  $T > T_c$  and  $T \ll T_c$ . We then use these normalization curves to obtain  $T'(T, \theta)$  at the same magnitude of  $H$  that rotates in the plane of the CDs. Once a value of  $B'$  at a given direction of the field is measured, the magnet is rotated by  $0.5^\circ$ , and the next point of the  $B'(\theta)$  curve is measured. Afterwards, by applying the mentioned normalization, we obtain the  $T'(\theta, H, T)$  curves. The transmittivity is

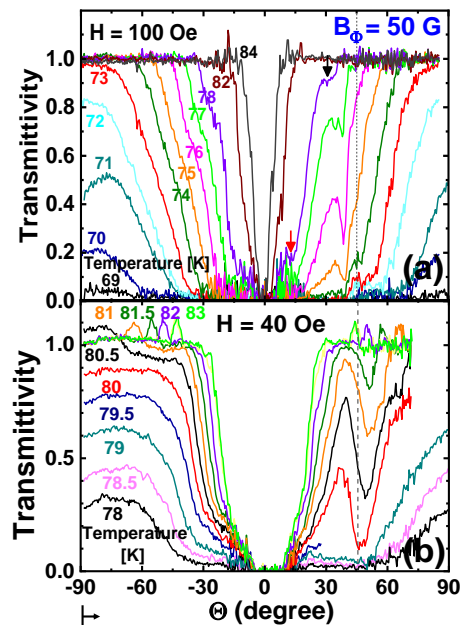


FIG. 3. Angular dependence of ac transmittivity  $T'$  for a  $\text{Bi}_2\text{Sr}_2\text{CaCu}_2\text{O}_{8+\delta}$  sample with tilted columnar defects (at  $45^\circ$  from the  $c$ -axis) and a density corresponding to  $B_\Phi = 50$  G.  $T'$  at various temperatures close to the melting line for applied fields of (a) 100 Oe and (b) 40 Oe. Positive (negative) angles correspond to the anti-clockwise (clockwise) direction from the  $ab$ -plane. The applied field is swept from the  $c$ -axis direction,  $\theta = 90^\circ$ , towards the  $ab$ -plane direction,  $\theta = 0^\circ$ , and beyond (see black arrow at the bottom left). Dashed lines indicate the direction of defects. Measurement temperatures are indicated using the same color code as the curves. The black arrow indicates the dip detected close to the direction of the columnar defects whereas the red one indicates a dip registered at a smaller angle.

a magnitude extremely sensitive to discontinuities in the local induction associated with first-order magnetic transitions such as, for instance, the vortex melting transition [35, 36]. In the  $T'$  angular measurements that we present here, we introduce an ac ripple field parallel to the  $c$ -axis on the background of an oblique dc field; namely, we measure the in-plane screening current affected by an out-of-plane dc field [35].

### III. RESULTS

The transmittivity versus temperature measurements performed with the field applied parallel to the  $c$ -axis reveal the presence of paramagnetic peaks; see the example of the top insert to Figure 2. The temperature-location of these peaks is independent of the frequency of the ripple field used to measure. In pristine samples, paramagnetic peaks with such phenomenology are considered indicative of the first-order melting transition since a peak in  $T'$  comes from a peak in  $B'$ , and then is the consequence

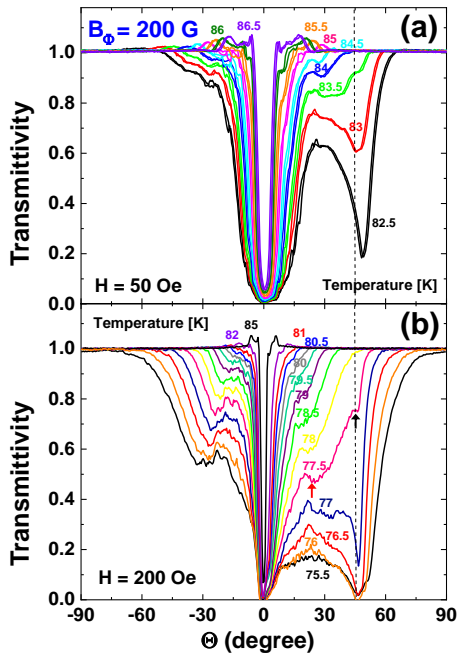


FIG. 4. Angular dependence of ac transmittivity  $T'$  for a  $\text{Bi}_2\text{Sr}_2\text{CaCu}_2\text{O}_{8+\delta}$  sample with tilted columnar defects (at  $45^\circ$  from the  $c$ -axis) and a density corresponding to  $B_\Phi = 200$  G.  $T'$  at various temperatures for applied fields of (a) 50 and (b) 200 Oe. Positive (negative) angles correspond to the anti-clockwise (clockwise) direction from the  $ab$ -plane. The applied field is swept from the  $c$ -axis direction,  $\theta = 90^\circ$ , towards the  $ab$ -plane direction,  $\theta = 0^\circ$ , and beyond. The dashed lines indicate the direction of the columnar defects. Labels corresponding to the temperatures are indicated with the same color code as the curves. The black arrow indicates the dip detected close to the direction of the columnar defects whereas the red one indicates a dip registered at a smaller angle.

of a jump in  $B$  [35, 37]. The location of these peaks in the field-temperature phase diagram is indicated with black dots in Figure 2 generating the  $H_{pp}$  line that indicates the location of the first-order solid-to-liquid vortex transition. The paramagnetic peaks in the  $B_\Phi = 50$  G sample are clearly detected down to 81 K and up to 40 Oe; for larger fields or smaller temperatures, we are not able to detect them due to the sudden decrease in  $T'$  associated with the screening in the vortex solid phase. These paramagnetic peaks are also resolved at high temperatures in the sample with  $B_\Phi = 200$  G.

Figure 3 shows angular-dependent transmittivity data, namely,  $T'$  vs.  $\theta$  for the  $B_\Phi = 50$  G sample at applied fields  $H$  of (a) 100 and (b) 40 Oe, and a ripple field of 0.7 Oe and 11 Hz. In this set of measurements, the paramagnetic peaks are clearly detected in the  $H = 40$  Oe case and appear more noisy in the  $H = 100$  Oe case. Figure 3b shows the succession of paramagnetic peaks close to the  $T' = 1$  value: they are located at smaller  $\theta$ , namely, smaller  $H^\perp$ , for larger temperatures. The peaks are roughly symmetrically detected at a given an-

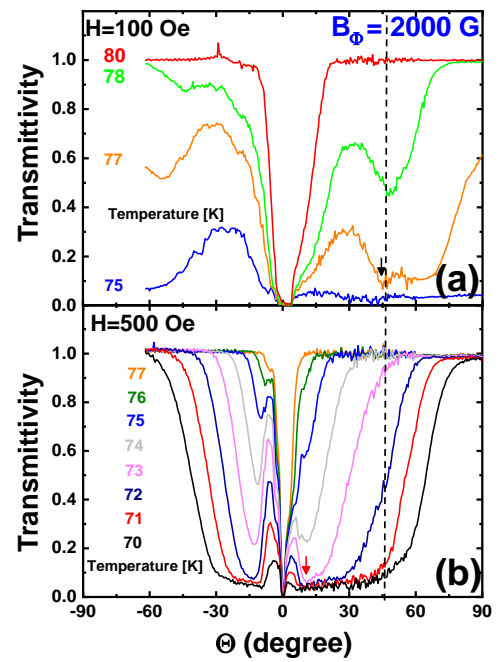


FIG. 5. Angular dependence of ac transmittivity  $T'$  for a  $\text{Bi}_2\text{Sr}_2\text{CaCu}_2\text{O}_{8+\delta}$  sample with tilted columnar defects (at  $45^\circ$  from the  $c$ -axis) and a density corresponding to  $B_\Phi = 2000$  G.  $T'$  at different temperatures for applied fields of (a) 100 and (b) 500 Oe. Positive (negative) angles correspond to the anti-clockwise (clockwise) direction from the  $ab$ -plane. The applied field is swept from the  $c$ -axis direction,  $\theta = 90^\circ$ , towards the  $ab$ -plane direction,  $\theta = 0^\circ$ , and beyond. The dashed lines indicate the direction of the columnar defects. Labels corresponding to the measurement temperatures are indicated with the same color code as the curves. The black arrow indicates the dip detected close to the direction of the columnar defects whereas the red one indicates a dip registered at a smaller angle.

gle  $\theta$  with respect to the  $ab$ -plane. Considering the value of the component  $H^\perp = H \sin \theta$  and the temperature at which these peaks are detected, we obtain the red dots shown in Figure 2 for  $H = 40$  Oe. These red points coincide with the  $H_{pp}$  black points. These results suggest that for a low density of CD, the relevant variable for the occurrence of the first-order transition in tilted fields for extremely anisotropic superconductors is the pancake vortex density, i.e., the  $c$ -axis component of the applied field. Thus, for a moderate CD density like  $B_\Phi = 50$  G, the nature of the first-order transition line detected at high temperatures in  $\text{Bi}_2\text{Sr}_2\text{CaCu}_2\text{O}_{8+\delta}$  is not significantly altered with respect to the case of pristine samples. Indeed, note that when comparing our results with those of Ref. [8], it is clear that the in-plane component is not large enough to produce a significant displacement of the field at which the transition occurs.

In the studied temperature range, the transmittivity vs.  $\theta$  curves are asymmetric with respect to both the  $ab$ -plane and the CD direction. This asymmetry is partly due to a ubiquitous feature in  $T'$ : a dip in the angles close

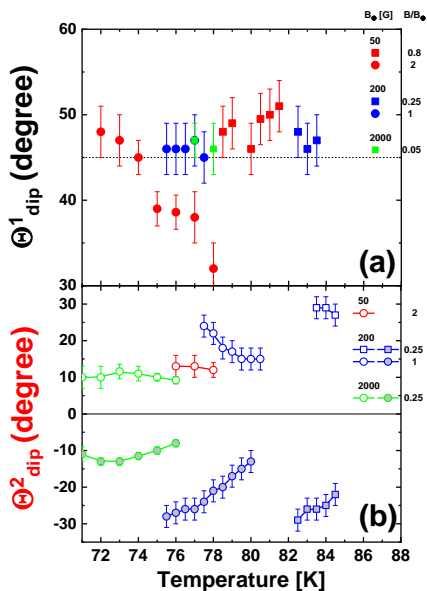


FIG. 6. Angular location of the dips in transmittivity for  $\text{Bi}_2\text{Sr}_2\text{CaCu}_2\text{O}_{8+\delta}$  samples with tilted columnar defects (at  $45^\circ$  from the  $c$ -axis) with densities corresponding to  $B_\Phi = 50$  (red points), 500 (blue points) and 2000 G (green points). Data are obtained from the curves of Figures 3 to 5 at various temperatures and different applied fields. The label indicates the ratio between the field applied to measure and the matching field,  $B/B_\Phi$ , namely, the vortex to CD number ratio. (a) Angular location of the dip in transmittivity detected close to the columnar defects direction,  $\Theta_{\text{dip}}^1$ . (b) Angular location of the sharper dips located at smaller angles  $\Theta_{\text{dip}}^2$  roughly symmetric with respect to the  $ab$ -plane.

but not exactly equal to the direction of CDs, visible only at positive angles. These dips are indicated with black arrows in Figures 3–5 for the three studied CD densities and appear at angles  $\Theta_{\text{dip}}^1$ . Local dips in ac transmittivity are associated with an enhancement of screening. The dips are observed at temperatures larger than 70 K, in a range of fields below and above  $B_\Phi$ . The angles  $\Theta_{\text{dip}}^1$  are larger than the ones at which we detect the paramagnetic peaks in the samples with  $B_\Phi = 50$  and 200 G associated to the first-order transition. Then, these dips occur for components  $H^\perp$  smaller than  $H_{\text{pp}}$ ; namely, this enhanced screening takes place within the solid vortex phase.

Figure 6 (a) summarizes the location of these dips for all the studied samples at different fields and temperatures. For vortex densities  $B/B_\Phi \leq 1$ , this enhancement of screening is detected close to, but not exactly aligned with, the direction of CD, namely,  $\Theta_{\text{dip}}^1 \sim 45^\circ$ . Then, this feature is quite possibly a manifestation of enhanced screening due to CD strongly pinning pancake vortices when the field is aligned close to the direction of defects. In the case when  $B/B_\Phi = 2$ , for temperatures greater than 75 K,  $\Theta_{\text{dip}}^1$  significantly decreases upon warming from the low-temperature  $\sim 45^\circ$  value.

The transmittivity curves for the three studied CD densities also present extra dips in  $T'$  that are generally

less pronounced than the ones located at  $\Theta_{\text{dip}}^1$ . These dips, indicated with red arrows in Figures 3, 4, and 5, are detected at angles  $|\Theta_{\text{dip}}^2| < 45^\circ$  for  $B/B_\Phi$  larger and greater than one. These dips are observed for positive as well as negative angles, appearing quite symmetric with respect to the  $\theta = 0$  direction; see Figure 6b for further details. In the case of the  $B_\Phi = 50$  G sample, the negative  $\Theta_{\text{dip}}^2$  values are not reported since the transmittivity curves are too noisy to provide a good estimation of this magnitude, though the dips at negative angles are faintly observed in the curves. Thus, the dips at  $\Theta_{\text{dip}}^2$  are a manifestation of an enhanced screening that occurs roughly symmetrically with respect to the  $ab$ -plane. In addition,  $|\Theta_{\text{dip}}^2|$  decreases upon increasing the temperature, concomitant with the dips becoming less pronounced upon warming.

#### IV. DISCUSSION

Tilted fields in extremely layered superconductors can give rise to a composite lattice phase where pancake vortices coexist with Josephson vortices, or to tilted chains of pancake vortices [3, 8]. A transition between both types of arrangements is reported by means of ac transmittivity measurements [8]. In our experimental data on the angular dependence of transmittivity, we explore a continuous set of ratios between in-plane and  $c$ -axis field components,  $H_{\parallel}/H_{\perp}$ . The dips in  $T'$  are detected within a  $H_{\parallel}/H_{\perp}$  range that does not coincide with the composite-to-tilted lattice transition experimentally reported in pristine  $\text{Bi}_2\text{Sr}_2\text{CaCu}_2\text{O}_{8+\delta}$  [8]. Therefore, the dips at  $\Theta_{\text{dip}}^1$  and  $\Theta_{\text{dip}}^2$  are not associated to this structural transition in vortex matter.

Another phenomenon relevant to tilted fields in layered superconductors is the so-called *lock-in* angle, which refers to the alignment of the vortex lattice with the  $ab$ -planes, creating a purely Josephson-vortex array [1, 38]. Considering the typical parameters for  $\text{Bi}_2\text{Sr}_2\text{CaCu}_2\text{O}_{8+\delta}$ , the lock-in angle where this arrangement is favorable should lie below  $2^\circ$ . This angle is much smaller than the ones at which the dips in  $T'$  are detected, and thus they cannot be associated to this phenomena either.

Therefore, the dips detected in our experimental range at  $\Theta_{\text{dip}}^1$  and  $\Theta_{\text{dip}}^2$  are more likely associated to a change in configuration between different arrangements within the composite lattice phase. The dips in  $T'$  are then the fingerprint of enhanced screening in a selected angular range associated to an improved pinning efficiency induced by the CD arrangement in the composite lattice phase. Since for  $B/B_\Phi \leq 1$  the magnitude of  $\Theta_{\text{dip}}^1 \sim 45^\circ$ , these dips are clearly related to pinning by the CD of a vortex arrangement made of tilted stacks of pancake vortices following the direction of CD that might eventually have a moderate deformation induced by the in-plane Josephson vortices. The fact that  $\Theta_{\text{dip}}^1$  is not exactly  $45^\circ$  degrees indicates that once this configuration is reached

at the vicinity of the CD direction upon increasing  $\theta$ , the system remains efficiently pinned by the defects even though the angle of the applied field continues increasing.

As mentioned, when  $B/B_\Phi > 1$ ,  $\Theta_{\text{dip}}^1$  significantly decreases upon warming from the low-temperature  $\sim 45^\circ$  value. This is an indication that for a larger density of vortices than that of CD, the system arranges in a configuration where only a fraction of the pancakes of individual vortices are pinned by CD and the rest lie outside of them. Then the fact that  $\Theta_{\text{dip}}^1$  decreases upon warming implies that the enhanced-screening configuration of the system occurs for a larger  $H_{\parallel}$  and then an increasing number of Josephson vortices. This is suggestive of not only CD but also Josephson vortices having a relevant role in determining the enhanced-screening configuration of the system and deserves further investigation.

As for the dips detected at  $\Theta_{\text{dip}}^2$ , since this angle is rather small, they seem to correspond to a staircase vortex configuration, where only a fraction of pancakes of individual vortices is tilted along the direction of CD. The more remarkable property of this feature is that the dips appear in pairs located almost symmetric with respect to the  $ab$ -plane direction. This is an indication that the enhanced screening in this angular range might be due to a combination of the pinning of CD with the pinning exerted by Josephson vortices that is symmetric with respect to the  $ab$ -plane. Another salient property of these dips is that the modulus of  $\Theta_{\text{dip}}^2$  decreases upon warming. This finding indicates, as in the case of  $\Theta_{\text{dip}}^1$ , that the enhanced-screening configuration of the system

occurs for a larger number of Josephson vortices upon warming.

## V. CONCLUSIONS

In conclusion, our angular transmittivity data in extremely layered  $\text{Bi}_2\text{Sr}_2\text{CaCu}_2\text{O}_{8+\delta}$  samples with tilted CD indicate that the screening of a ripple field is enhanced when the vortex direction is around that of CDs but an extra enhancement of screening is detected at small angles, almost symmetric with the  $ab$ -plane direction. This particular angularly selective enhanced screening has not been reported in other superconductors and arises due to the efficiency of CDs in pinning a composite lattice of vortices nucleated in an extremely layered material in tilted fields. For directions close to the CD, as expected, pancake vortices profit at maximum pinning, being located at the defects. Strikingly, screening is also enhanced at smaller angles where the composite lattice is efficiently pinned, probably by adjusting itself into a staircase configuration to take better advantage of the pinning landscape.

This research was funded by the National Council of Scientific and Technical Research of Argentina (CONICET) through grant PIP 2021-1848, by the Argentinean Agency for the Promotion of Science and Technology (ANPCyT) through grant PICT 2017-2182, and by the Universidad Nacional de Cuyo research Grant 06/C008-T1.

- 
- [1] Blatter, G.; Feigel'mann, M.V.; Geshkenbein, V.B.; Larkin, A.I.; Vinokur, V.M. Vortices in high-temperature superconductors. *Rev. Mod. Phys.* **1994**, *66*, 1125–1388.
  - [2] Bending, S.J.; Dodgson, M.J.W. Vortex Chains in Anisotropic Superconductors. *J. Condens. Matter Phys.* **2005**, *17*, R955.
  - [3] Koshelev, A.E. Vortex-chain phases in layered superconductors. *Phys. Rev. B* **2005**, *71*, 174507.
  - [4] Clem, J.R. Two-dimensional vortices in a stack of thin superconducting films: A model for high-temperature superconducting multilayers. *Phys. Rev. B* **1991**, *43*, 7837–7846.
  - [5] Bulaevskii, L.N.; Ledvij, M.; Kogan, V.G. Vortices in layered superconductors with Josephson coupling. *Phys. Rev. B* **1992**, *46*, 366–380.
  - [6] Koshelev, A.E. Crossing Lattices, Vortex Chains, and Angular Dependence of Melting Line in Layered Superconductors. *Phys. Rev. Lett.* **1999**, *83*, 187–190.
  - [7] Koshelev, A.E.; Latyshev, Y.I.; Konczykowski, M. Slowing down the Josephson vortex lattice in  $\text{Bi}_2\text{Sr}_2\text{CaCu}_2\text{O}_{8+\delta}$  with pancake vortices. *Phys. Rev. B* **2006**, *74*, 104509.
  - [8] Konczykowski, M.; van der Beek, C.J.; Koshelev, A.E.; Mosser, V.; Dodgson, M.; Kes, P.H. Composite to Tilted Vortex Lattice Transition in  $\text{Bi}_2\text{Sr}_2\text{CaCu}_2\text{O}_{8+\delta}$  in Oblique Fields. *Phys. Rev. Lett.* **2006**, *97*, 237005.
  - [9] Bolle, C.A.; Gammel, P.L.; Grier, D.G.; Murray, C.A.; Bishop, D.J.; Mitzi, D.B.; Kapitulnik, A. Observation of a commensurate array of flux chains in tilted flux lattices in Bi-Sr-Ca-Cu-O single crystals. *Phys. Rev. Lett.* **1991**, *66*, 112–117.
  - [10] Grigorieva, I.V.; Steeds, J.W.; Balakrishnan, G.; Paul, D.M. Vortex-chain state in  $\text{Bi}_2\text{Sr}_2\text{CaCu}_2\text{O}_{8+\delta}$ : Experimental evidence for coexistence of two vortex orientations. *Phys. Rev. B* **1995**, *51*, 3765–3772.
  - [11] Vlasko-Vlasov, V.K.; Koshelev, A.; Welp, U.; Crabtree, G.W.; Kadowaki, K. Decoration of Josephson vortices by pancake vortices in  $\text{Bi}_2\text{Sr}_2\text{CaCu}_2\text{O}_{8+\delta}$ . *Phys. Rev. B* **2002**, *66*, 014523.
  - [12] Tokunaga, M.; Tamegai, T.; Fasano, Y.; de la Cruz, F. Direct observations of the vortex chain state in  $\text{Bi}_2\text{Sr}_2\text{CaCu}_2\text{O}_{8+y}$  by Bitter decoration. *Phys. Rev. B* **2003**, *67*, 134501.
  - [13] Vlasko-Vlasov, V.K.; Glatz, A.; Koshelev, A.E.; Welp, U.; Kwok, W.K. Anisotropic superconductors in tilted magnetic fields. *Phys. Rev. B* **2015**, *91*, 224505.
  - [14] Correa, V.F.; Kaul, E.E.; Nieva, G. Overdoping effects in  $\text{Bi}_2\text{Sr}_2\text{CaCu}_2\text{O}_{8+y}$ : From electromagnetic to Josephson interlayer coupling. *Phys. Rev. B* **2001**, *63*, 172505.
  - [15] Civale, L., Marwick, A. D., Worthington, T. K., Kirk, M. A., Thompson, J. R., Krusin-Elbaum, L., Sun, Y., Clem, J. R., and Holtzberg, F., Vortex Confinement by

- Columnar Defects in  $\text{YBa}_2\text{Cu}_3\text{O}_7$  Crystals: Enhanced Pinning at High Fields and Temperatures, *Phys. Rev. Lett.* **1991**, *67*, 648–652.
- [16] Thompson, J. R., Sun, Y. R., Kerchner, H. R., Christen, D. K., Sales, B. C., Chakoumakos, B. C., Marwick, A. D., Civale, L. and Thomson, J. O. Enhanced current density  $J_c$  and extended irreversibility in single-crystal  $\text{Bi}_2\text{Sr}_2\text{Ca}_1\text{Cu}_2\text{O}_8$  via linear defects from heavy ion irradiation, *Appl. Phys. Lett.* **1992**, *60*, 2306–2313.
- [17] Thompson, J. R., Krusin-Elbaum, L., Civale, L., Blatter, G., and Feild, C. Superfast vortex creep in  $\text{YBa}_2\text{Cu}_3\text{O}_7$  crystals with columnar defects: evidence for variable-range vortex hopping, *Phys. Rev. Lett.* **1997**, *78*, 3181–3184.
- [18] Silhanek, A., Niebieskikwiat, D., Civale, L., Avila, M. A., Billoni, O., and Casa, D. Anomalous behavior of the irreversible magnetization and time relaxation in  $\text{YBa}_2\text{Cu}_3\text{O}_7$  single crystals with splayed tracks, *Phys. Rev. B* **1999**, *60*, 13189–13195.
- [19] Ta Phuoc, V., Olive, E., De Sousa, R., Ruyter, A., Ammor, L., and Soret, J. C. Response to Tilted Magnetic Fields in  $\text{Bi}_2\text{Sr}_2\text{CaCu}_2\text{O}_{8+y}$  with Columnar Defects: Evidence for Transverse Meissner Effect, *Phys. Rev. Lett.* **2002**, *88*, 187002–1–4.
- [20] Ammor, L., Pignon, B., Hong, N. H., and Ruyter, A. Angle-resolved I-V characteristics measurements in  $\text{Bi}_{1.8}\text{Pb}_{0.2}\text{Sr}_2\text{CaCu}_2\text{O}_{8+\delta}$  single crystals with inclined columnar defects, *Phys. Rev. B* **2004**, *69*, 224511–1–9.
- [21] Kwok, W.-K., Welp, U., Glatz, A., Koshelev, A. E., Kihlstrom, K. J., and Crabtree, G. W. Vortices in high-performance high-temperature superconductors, *Rep. Prog. Phys.* **2016**, *79*, 116501–1–39.
- [22] Verdene, T.; Beidenkopf, H.; Myasoedov, Y.; Shtrikman, H.; Rappaport, M.; Zeldov, E.; Tamegai, T. Multiple Changes of Order of the Vortex Melting Transition in  $\text{Bi}_2\text{Sr}_2\text{CaCu}_2\text{O}_{8+\delta}$  with Dilute Columnar Defects. *Phys. Rev. Lett.* **2008**, *101*, 157003.
- [23] Tonomura, A., Kasai, H., Kamimura, O., Matsuda, T., Harada, K., Nakayama, Y., Shimoyama, J., Kishio, K., Hanaguri, T., Kitazawa, K., Sasase, M., and Okayasu, S. Observation of individual vortices trapped along columnar defects in high-temperature superconductors, *Nature*, **2001**, *412*, 620–622..
- [24] Dai, H., Yoon, S., Liu, J., Budhani, R. C., and Lieber, C. Simultaneous Observation of Columnar Defects and Magnetic Flux Lines in High-Temperature  $\text{Bi}_2\text{Sr}_2\text{CaCu}_2\text{O}_8$  Superconductors, *Science*, **1994**, *265*, 1552–4.
- [25] Cejas Bolecek, N. R., Kolton, A.B., Konczykowski, M., Pastoriza, H., Domínguez, D., and Fasano, Y. Vortex matter freezing in  $\text{Bi}_2\text{Sr}_2\text{CaCu}_2\text{O}_8$  samples with a very dense distribution of columnar defects, *Phys. Rev. B*, **2016**, *93*, 054505–1–10.
- [26] Hebert, S.; Hardy, V.; Villard, G.; Hervieu, M.; Simon, C.; Provost, J. Vortex pinning by different angular distributions of columnar defects in  $\text{Bi}_2\text{Sr}_2\text{CaCu}_2\text{O}_8$ . *Phys. Rev. B* **1998**, *57*, 649–655.
- [27] Ishikawa, N.; van der Beek, C.J.; Dunlop, A.; Jaskierowicz, G.; Li, M.; Kes, P.H.; Della-Negra, S. Vortex phase diagram in  $\text{Bi}_2\text{Sr}_2\text{CaCu}_2\text{O}_{8+\delta}$  with damage tracks created by 30 MeV fullerene irradiation. *J. Phys. Soc. Jpn.* **2004**, *73*, 2813–2822.
- [28] Schuster, T.; Kuhn, H.; Indenbom, M.V.; Kreiselmeyer, G.; Leghissa, M.; Klaumanzer, S. Direct observation of stronger flux-line pinning of crossed compared to parallel linear defects. *Phys. Rev. B* **1996**, *57*, 2257–2260.
- [29] Hebert, S.; Perkins, G.; Abd el-Salam, M.; Caplin, A.D. Interplay between two families of columnar defects in  $\text{Bi}_2\text{Sr}_2\text{CaCu}_2\text{O}_8$  single crystals. *Phys. Rev. B* **2000**, *62*, 15230–15236.
- [30] Kato, T.; Shibauchi, T.; Matsuda, Y.; Thompson, J.R.; Krusin-Elbaum, L. Entanglement of Solid Vortex Matter: A Boomerang-Shaped Reduction Forced by Disorder in Interlayer Phase Coherence in  $\text{Bi}_2\text{Sr}_2\text{CaCu}_2\text{O}_{8+y}$ . *Phys. Rev. Lett.* **2008**, *101*, 027003.
- [31] Silhanek, A.; Civale, L.; Candia, S.; Nieva, G.; Pasquini, G.; Lanza, H. Evidence for vortex staircases in the whole angular range due to competing correlated pinning mechanisms. *Phys. Rev. B* **1999**, *59*, 13620–13623.
- [32] van der Beek, C.J.; Konczykowski, M.; Vinokur, V.M.; Crabtree, G.W.; Li, T.W.; Kes, P.H. Vortex dynamics in a  $\text{Bi}_2\text{Sr}_2\text{CaCu}_2\text{O}_8$  crystal with columnar defects. *Phys. Rev. B* **1995**, *51*, 15492–15505.
- [33] van der Beck, C.J.; Konczykowski, M.; Samoilov, A.V.; Chikumoto, N.; Bouffard, S.; Feigelman, M.V. Defect-Unbinding and the Bose-Glass Transition in Layered Superconductors. *Phys. Rev. Lett.* **2001**, *86*, 5136–5139.
- [34] Li, T.W.; Kes, P.H.; Hien, N.T.; Franse, J.J.M.; Menovsky, A.A. Growth of  $\text{Bi}_2\text{Sr}_2\text{CaCu}_2\text{O}_{8+x}$  single crystals at different oxygen ambient pressures. *J. Cryst. Growth* **1994**, *135*, 481–486.
- [35] Dolz, M.I.; Fasano, Y.; Pastoriza, H.; Mosser, V.; Li, M.; Konczykowski, M. Latent heat and nonlinear vortex liquid in the vicinity of the first-order phase transition in layered high- $T_c$  superconductors. *Phys. Rev. B* **2014**, *90*, 144507.
- [36] Dolz, M.I.; Fasano, Y.; Cejas Bolecek, N.R.; Pastoriza, H.; Mosser, V.; Li, M.; Konczykowski, M. Size-induced depression of first-order transition lines and entropy jump in extremely layered nanocrystalline vortex matter. *Phys. Rev. Lett.* **2015**, *115*, 137003.
- [37] Schmidt, B.; Konczykowski, M.; Morozov, N.; Zeldov, E. Angular dependence of the first-order vortex-lattice phase transition in  $\text{Bi}_2\text{Sr}_2\text{CaCu}_2\text{O}_8$ . *Phys. Rev. B* **1997**, *55*, R8705–R8708.
- [38] Feinberg, D.; Villard, C. Intrinsic pinning and lock-in transition of flux lines in layered type-II superconductors. *Phys. Rev. Lett.* **1990**, *65*, 919–922.